Optimal control of piezophotonic and magnetophotonic switching in a dense medium of three-level atoms

Ningjun Wang and Herschel Rabitz
Department of Chemistry, Princeton University, Princeton, New Jersey 08544

Aaron S. Manka and Charles M. Bowden
Weapons Sciences Directorate, AMSMI-RD-WS-ST, Research, Development, and Engineering Center, U.S. Army Missile Command, Redstone Arsenal, Alabama 35898-5248

(Received 27 October 1995)

We apply optimal control techniques to maximize the absorptionless index of refraction, the density-dependent piezophotonic switching between absorption and amplification, and the ground-state energy-level-spacing-dependent magnetophotonic switching of susceptibility in a dense medium of coherently prepared three-level systems.

PACS number(s): 42.50.−p

Quantum coherence and interference can lead to many interesting optical phenomena, such as electromagnetically-induced transparency (EIT) [1], lasing without inversion (LWI) [2,3], and large index of refraction without absorption [4]. In a dense medium, the near dipole-dipole (NDD) interactions become significant and have to be taken into account properly [5–7]. It was shown that the NDD interactions can enhance the inversionless gain and absorptionless index of refraction, and lead to a density-dependent switching between absorption and amplification [8]. However, it is very difficult to optimize in a straightforward manner due to the large dimensionality of the parameter space. The optimal control technique (OCT), however, has been employed to manipulate atomic coherence and interference to achieve various goals, e.g., designing optical pulse shapes to control EIT [9], LWI [10], and atomic population transfer [11]. Here we apply it to design material parameters to enhance the absorptionless index of refraction and optical switching effects.

We investigate a medium composed of an atomic beam of three-level atoms. An energy-level scheme of the atoms is shown in the inset of Fig. 1. The lower two levels, which may correspond to a magnetic degeneracy, are closely spaced and initially prepared in a coherent superposition state. The atomic preparation can be accomplished by a coherent pulse, e.g., a microwave field just before these atoms are injected into an interaction region of volume V at an injection rate r. A probe field E couples the upper level to the coherent superposition of the two lower levels. Using the rotating-wave approximation, the equations of motion for the density-matrix elements are [8]

$$\dot{\rho}_{aa}=r\rho_{aa}^{0}-\gamma_a\rho_{aa}-(i/\hbar)[(\mu\rho_{ba}+\mu'\rho_{b'a})E_L-\text{c.c.}], \tag{1a}$$

$$\dot{\rho}_{b'b'}=r\rho_{b'b'}^{0}-\gamma_{b'}\rho_{b'b'}-(i/\hbar)(\mu'\rho_{ab'}E_L^{*}-\text{c.c.}), \tag{1b}$$

$$\dot{\rho}_{bb}=r\rho_{bb}^{0}-\gamma_b\rho_{bb}-(i/\hbar)(\mu\rho_{ab}E_L^{*}-\text{c.c.}), \tag{1c}$$

$$\dot{\rho}_{ab'}=-(\gamma_{ab'}+i\Delta_{ab'})\rho_{ab'}-(i/\hbar)\mu'(\rho_{b'b'}-\rho_{aa})E_L-(i/\hbar)\mu\rho_{bb'}E_L, \tag{1d}$$

$$\dot{\rho}_{ab}=-(\gamma_{ab}+i\Delta_{ab})\rho_{ab}-(i/\hbar)\mu(\rho_{bb}-\rho_{aa})E_L-(i/\hbar)\mu'\rho_{b'b}E_L, \tag{1e}$$

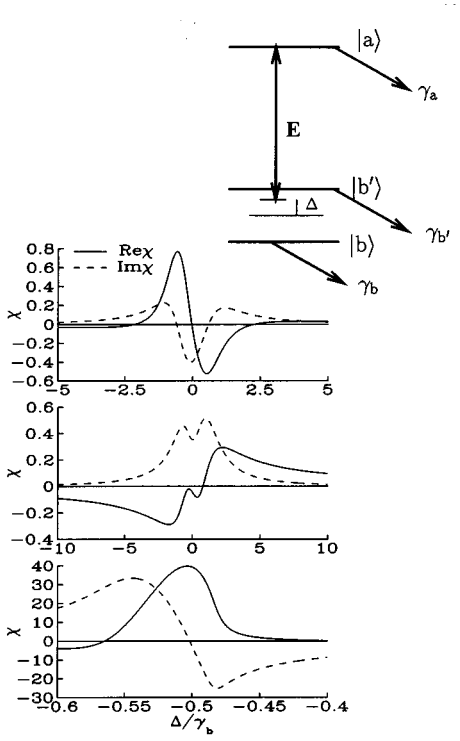

FIG. 1. Reχ (solid line) and Imχ (dashed line) as functions of detuning Δ. Positive and negative Imχ correspond to absorption and amplification, respectively. Upper and middle panels are obtained using the initial trial parameter (set 0 of Table I) with $\gamma_a=0.05\gamma_b$ and γ_b, respectively. The lower panel is obtained using optimal parameters that minimize J_1 (set 1 of Table I) with $\gamma_a=\gamma_b$. Inset: A schematic energy-level diagram of the three-level system.

$$\dot{\rho}_{b'b}=r\rho^0_{b'b}-(\gamma_{b'b}+i\omega_{b'b})\rho_{b'b}-(i/\hbar)(\mu'\rho_{ab}E_L^*-\mu\rho_{b'a}E_L), \tag{1f}$$

where ρ^0_{ij} are the elements of the initial density matrix of an injected atom, with $\rho^0_{aa}+\rho^0_{bb}+\rho^0_{b'b'}=1$. Here μ' and μ are the dipole matrix elements (assumed real) of $|a\rangle\rightarrow|b'\rangle$ and $|a\rangle\rightarrow|b\rangle$ transitions, respectively, $\Delta_{ij}\equiv\omega_{ij}-\nu$, where ν is the probe-field frequency $(i,j=a,b',b)$. We also define γ_i as the decay rates out of the various levels and $\gamma_{ij}=(\gamma_i+\gamma_j)/2$ as the dephasing rate of the corresponding transitions. The detuning from the center of the lower two energy levels is defined as $\Delta\equiv\Delta_{ab'}+\omega_{b'b}/2=\Delta_{ab}-\omega_{b'b}/2$ (see the inset of Fig. 1).

In Eq. (1), E_L is the local microscopic field that is related to the macroscopic field E through the Lorentz-Lorenz relation, $E_L=E+P/3\epsilon_0$. Here $P=-(\mu\rho_{ab}+\mu'\rho_{ab'})/V$ is the volume polarization of an isotropic, homogeneous, dense medium.

The density-dependent parameter C, which is a measure of the strength of the NDD interaction and nonlinearity [8] in the system, is defined as

$$C=\frac{N\mu^2}{2\varepsilon_0\hbar\gamma_b}, \tag{2}$$

where $N=(r/\gamma_b)/V$ is the effective atomic density in the interaction volume V.

The macroscopic susceptibility that accounts for NDD interaction is given by [8]

$$\chi\equiv\frac{P}{\epsilon_0 E}=\frac{\chi_e}{1-\chi_e/3}, \tag{3}$$

where $\chi_e\equiv P/(\epsilon_0E_L)=-(\mu\rho_{ab}+\mu'\rho_{ab'})/(V\epsilon_0E_L)$ is the susceptibility with respect to the local field and can be obtained numerically by solving the linear equations (1) for ρ_{ij} with $\dot{\rho}_{ij}=0$ (steady state). We find that χ_e depends on the parameters $I_L=|\mu E_L/\hbar|^2$, Δ, $\omega_{b'b}$, and $C\rho^0_{ij}$. The local-field intensity I_L is not an observable, but is related to the macroscopic-field intensity $I=|\mu E/\hbar|^2$ (an observable) by the nonlinear equation [8]

$$I_L|1-\tfrac{1}{3}\chi_e(I_L,\Delta,\omega_{b'b},C\rho^0_{ij})|^2=I. \tag{4}$$

The susceptibility χ can be obtained numerically as follows: for a given set of control parameters I, Δ, $\omega_{b'b}$, $C\rho^0_{ij}$, find the root of Eq. (4) for I_L, calculate χ_e, and then substitute it into Eq. (3) to obtain χ. In this way, we can obtain $\chi(I,\Delta,\omega_{b'b},C\rho^0_{ij})$ numerically as a function of controllable parameters. The nonlinear equation (4) may have multiple roots, which leads to multistability.

To demonstrate the power and usefulness of the OCT, we examine the particular case of large, near-resonant, absorptionless index of refraction that was first predicted by Scully [4] for this system. However, in previous works [4,8], the upper-level decay rate γ_a is chosen to be $0.05\gamma_b$, which is significantly smaller than the lower-level decay rate γ_b. This yields a maximum of the refractive index at a point of zero loss (upper panel of Fig. 1). However, we believe that it is more realistic for γ_a to have the same order of magnitude as γ_b. We therefore set $\gamma_a=\gamma_b$ in all our numerical calculations. Unfortunately, for these parameters, we see from the middle panel of Fig. 1 that the system now shows broadband losses with reduced refractive index. We now employ the OCT to maximize $\mathrm{Re}\chi$ while simultaneously minimizing $\mathrm{Im}\chi$ at a desired probe detuning Δ, which can be achieved by minimizing the following objective functions:

TABLE I. Set 0 is the initial trial parameters that lead to set 1. Set 1 is the optimal parameters outside the bistable region for large index of refraction without absorption, i.e., the parameters that minimize J_1. We have assumed $\rho^0_{b'b'}=\rho^0_{bb}=(1-\rho^0_{aa})/2$.

Set	I	ρ^0_{aa}	ϕ	$\omega_{b'b}$	C
0	10^{-2}	0.01	$3\pi/2$	1	1
1	10^{-4}	0.2072	5.1503	1.0942	16.616

$$J_1=\beta_1\mathrm{Im}\chi(I,\Delta,\omega_{b'b},C\rho^0_{ij})-\beta_2\mathrm{Re}\chi(I,\Delta,\omega_{b'b},C\rho^0_{ij}), \tag{5}$$

where β_1 and β_2 are non-negative weight constants. Setting $\beta_1\ll\beta_2$ is equivalent to desiring a maximum index of refraction regardless of the value of absorption, while setting $\beta_1\gg\beta_2$ is equivalent to desiring a minimum absorption regardless of the value of index. Note that the control parameters must satisfy the constraints $C\rho^0_{ii}\geq0$, $i=a,b,b'$, $|\rho^0_{b'b}|=\sqrt{\rho^0_{bb}\rho^0_{b'b'}}$, and $I\geq I_{\min}$, where $I_{\min}$ is the minimum intensity feasible in the laboratory. It is therefore convenient to introduce real quantities Ω, ρ_i, and ϕ defined as $I=I_{\min}+\Omega^2$, $C\rho^0_{ii}\equiv\rho_i^2$, and $C\rho^0_{b'b'}=\rho_b\rho_{b'}e^{i\phi}$ so that the constraints on I and ρ^0_{ij} are automatically satisfied. We then optimize the new parameters Ω, $\omega_{b'b}$, ρ_i, ϕ using the steepest descent algorithm. Since levels b and b' are very close, it is a good approximation to assume that $\rho^0_{bb}=\rho^0_{b'b'}$ and $\mu=\mu'$. However, our optimal control algorithm is not limited by this. In all numerical calculations, we choose (unless otherwise stated) $\Delta=-0.5$, $\beta_1=0$, $\beta_2=1$, $I_{\min}=10^{-4}$, and $\gamma_a=\gamma_b=\gamma_{b'}=1$ as the unit of frequency.

We find that the optimal parameters that minimize J_1 lie in the bistable region. To avoid the bistability, we terminate the program just before the parameters enter the bistable region. Thus, we obtain the optimal parameters outside the bistable region, which are given in Table I (set 1). Parameter set 0 is the initial trial parameters used by the steepest-descent algorithm. The lower panel of Fig. 1 shows that the absorptionless index of refraction is recovered (at $\Delta=-0.5$) whose magnitude is enhanced by 50 times (compared with upper panel) with a comparable enhancement in peak gain.

We now apply the OCT to optimize the piezophotonic switching effect, whereby the system switches from amplification to absorption for a small change in density-dependent parameter C, which was first predicted by Manka *et al.* [8]. In that work, the choice is made that $\gamma_a=0.05\gamma_b$, which is much smaller than γ_b. We have confirmed that if γ_a is increased by a small amount, e.g., $\gamma_a=0.0504\gamma_b$, with other parameters unchanged, then $\mathrm{Im}\chi$ is positive for all C and thus the piezophotonic switching effect vanishes.

In this paper, we choose $\gamma_a=\gamma_b$, which is more realistic, and we will use the OCT to recover and enhance the piezophotonic switching effect. In addition, we set the lower

TABLE II. Set 0 contains the initial trial parameters that lead to sets 1 and 2. Set 1 contains the optimal parameters for piezophotonic switching, i.e., the parameters that minimize J_2 with $\lambda=1.05$. Set 2 contains the optimal parameters for threshold magnetophotonic switching, i.e., the parameters that minimize J_3 with $\lambda=1.04$. Set 3 contains the optimal parameters for usual magnetophotonic switching, i.e., the parameters that minimize J_4 with $\lambda=1.02$. The initial trial parameters that lead to set 3 are the same as set 0 except $I=10^{-3}$, $\omega_{b'b}=0.89$. We have assumed $\rho^0_{b'b'}=\rho^0_{bb}=(1-\rho^0_{aa})/2$.

Set	I	ρ^0_{aa}	ϕ	$\omega_{b'b}$	C
0	10^{-2}	0.16	$3\pi/2$	1	18.5
1	10^{-4}	0.1599	4.794	0.9784	19.471
2	10^{-4}	0.1693	4.8422	0.9332	19.599
3	1.2366×10^{-3}	0.1666	4.7456	0.8694	19.066

bound of the probe field to $I_{\min}=10^{-4}$, which is larger than the probe-field intensity 2.205×10^{-5} chosen in Ref. [8]. For field strengths of this magnitude, it is more difficult to enhance the piezophotonic switching effect, since a large field intensity will wash out the coherence of the lower two levels and reduce the enhancement. To enhance the piezophotonic switching effect, we construct the following objective functional:

$$J_2=\mathrm{Im}\chi(I,\Delta,\omega_{b'b},C\rho^0_{ij})\mathrm{Im}\chi(I,\Delta,\omega_{b'b},\lambda C\rho^0_{ij}). \quad (6)$$

We want to switch $\mathrm{Im}\chi$ from being large positive to large negative (or the reverse) when C is changed by a factor of λ (we choose $\lambda=1.05$ in our numerical calculation). This can be achieved by minimizing J_2.

The optimal set of parameters is shown in Table II (set 1). We plot $\mathrm{Im}\chi(\Delta)$ as a function of C using these optimal parameters in Fig. 2 (solid and dashed line). The solid and dashed lines correspond to the stable and unstable steady states, respectively. The solid line has a much larger slope across zero compared with the dotted line, which corresponds to the initial trial parameter (set 0 of Table II) used by the steepest-descent algorithm. Therefore the piezophotonic switching effect is significantly enhanced after optimization. The slope of the solid line across zero is also enhanced by a factor of 1.45 compared with that of Ref. [8]. This is quite respectable considering that we have used a much larger upper-level decay rate and field strength.

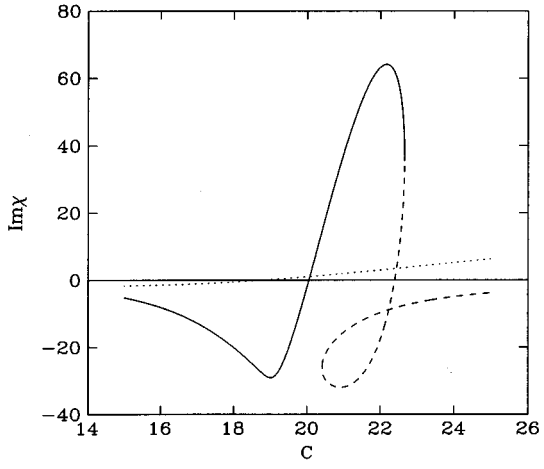

FIG. 2. $\mathrm{Im}\chi(\Delta=-0.5)$ as a function of C showing the piezophotonic switching effect. Positive and negative $\mathrm{Im}\chi$ correspond to absorption and amplification, respectively. Solid and dashed lines are the results of optimal parameters that minimize J_2 (set 1 of Table II). Solid and dashed lines denote stable and unstable steady states, respectively. The dotted line is the result of initial trial parameters (set 0 of Table II).

In the bistable region $20.42\leqslant C\leqslant 22.66$ there are three distinct steady states, but only one of them is stable and is indicated by a solid line. The figure also shows that $C=22.66$ is the instability threshold beyond which there is no stable steady state. This condition is somewhat similar to recent work on the dynamics of a single-mode inhomogeneously broadened laser [12], which showed that the NDD interactions lead to instabilities and chaos at much lower pumping levels. To fully understand the behavior of the system for $C>22.66$, the dynamic density-matrix equation (1) must be solved, which is beyond the scope of this paper.

In Table I (set 1) and Table II (set 1), optimal values of I are equal to $I_{\min}=10^{-4}$. This means that in order to maximize absorptionless index of refraction and piezophotonic switching effects, one should use the smallest achievable field intensity. We have repeated the optimization leading to Fig. 2 with larger $I_{\min}$ and found that the slope of $\mathrm{Im}\chi$ across zero decreases. This confirms the intuition that strong fields wash out the coherence of the lower two levels and reduce the enhancement.

Instead of varying C, one can obtain optical switching by varying $\omega_{b'b}$ as well; that is, the system switches from large

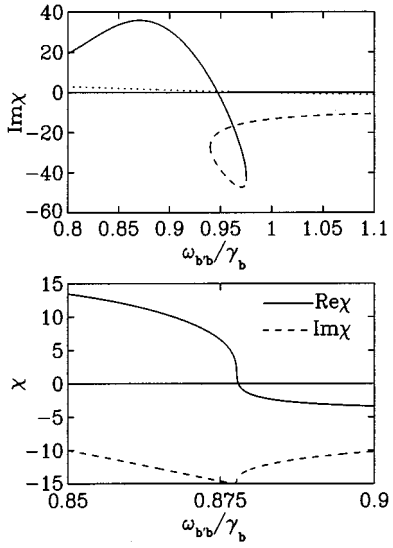

FIG. 3. Upper panel: $\mathrm{Im}\chi(\Delta=-0.5)$ as a function of $\omega_{b'b}$ showing threshold magnetophotonic switching. Positive and negative $\mathrm{Im}\chi$ correspond to absorption and amplification, respectively. Solid and dashed lines are obtained with the optimal parameters that minimize J_3 (set 2 of Table II). Here solid and dashed lines denote stable and unstable steady states, respectively. The dotted line is obtained using initial trial parameters (set 0 of Table II). Lower panel: $\mathrm{Re}\chi(\Delta=-0.5)$ (solid line) and $\mathrm{Im}\chi(\Delta=-0.5)$ (dashed line) as functions of $\omega_{b'b}$ for the optimal parameters outside the bistable region that minimize J_4 (set 3 of Table II). The figure shows the usual magnetophotonic switching in the presence of gain.

absorption to large gain (or the reverse) for a small change in the level spacing $\omega_{b'b}$. Since $\omega_{b'b}$ may be controlled by a dc magnetic field, we will call this magnetophotonic switching, which can be exploited to build a threshold magnetometer. To achieve this, we minimize the following objective functional:

$$J_3 = \mathrm{Im}\chi(I,\Delta,\omega_{b'b},C\rho_{ij}^0)\mathrm{Im}\chi(I,\Delta,\lambda\omega_{b'b},C\rho_{ij}^0). \quad (7)$$

We choose $\lambda=1.04$. Again we use set 0 of Table II as the initial trial parameters. The optimal parameters are shown in Table II (set 2). The upper panel of Fig. 3 displays $\mathrm{Im}\chi$ as a function of $\omega_{b'b}$ using the optimal parameters (solid and dashed lines). Here, as before, the dashed line indicates the unstable state. The solid line has a much larger slope across zero compared with the dotted line, which corresponds to the initial trial parameter (set 0). This means that the magnetophotonic switching effect is significantly enhanced after optimization. Note that $\omega=0.9754$ is the instability threshold beyond which there is no stable steady state.

Usually, a magnetometer's sensitivity is based on a large slope of refractive index ($\mathrm{Re}\chi$) that crosses through zero. This slope is essential to the phase measurements in an interferometer-type device [13]. To enhance this slope, we minimize the following objective functional:

$$J_4 = \mathrm{Re}\chi(I,\Delta,\omega_{b'b},C\rho_{ij}^0)\mathrm{Re}\chi(I,\Delta,\lambda\omega_{b'b},C\rho_{ij}^0), \quad (8)$$

with $\lambda=1.02$. We found that the optimal parameters are in the bistable region, which result in $\mathrm{Re}\chi$ jumping discontinuously from positive to negative for an infinitesimal change of $\omega_{b'b}$. A phase-sensitive magnetometer, however, is based on continuous and rapid change of $\mathrm{Re}\chi$ with a magnetic field instead of a discontinuous jump. We therefore limit the program to parameters outside the bistable region. We then obtain the optimal parameters that are just outside the bistable region (Table II set 3). We have used the initial trial parameters shown in set 0 except $I=10^{-3}$ and $\omega_{b'b}=0.89$. We display $\mathrm{Re}\chi(\omega_{b'b})$ (solid line) and $\mathrm{Im}\chi(\omega_{b'b})$ (dashed line) for the optimal parameters in the lower panel of Fig. 3. It is remarkable that optimal $\mathrm{Re}\chi$ changes continuously from positive to negative with almost infinite slope across zero and with gain ($\mathrm{Im}\chi<0$). This is ideal for a magnetometer.

In conclusion, we have applied the OCT to design material parameters to maximize the absorptionless index of refraction and the piezophotonic switching. We are able to enhance these effects for a more realistic upper-level decay rate, which is of the same order of magnitude as the lower-level decay rate. We have also reported here the magnetophotonic switching effect due to the NDD interactions, as well as the enhancement using the OCT. To that end, we obtain $\mathrm{Re}\chi$ that changes continuously across zero with almost infinite slope and with gain.

We (N.W. and H.R.) acknowledge financial support from the U.S. Army Research Office and one of us (A.S.M.) acknowledges the National Research Council for financial support.

[1] S. E. Harris, Phys. Rev. Lett. **70**, 552 (1993); **72**, 52 (1994).
[2] S. E. Harris, Phys. Rev. Lett. **62**, 1033 (1989).
[3] A. Nottelmann, C. Peters, and W. Lange, Phys. Rev. Lett. **70**, 1783 (1993); E. S. Fry *et al.*, *ibid.* **70**, 3235 (1993); W. E. van der Veer, R. J. J. van Diest, A. Dönszelmann, and H. B. van Linden van den Heuvell, *ibid.* **70**, 3243 (1993).
[4] M. O. Scully, Phys. Rev. Lett. **67**, 1855 (1991); M. Fleischhauer *et al.*, Phys. Rev. A **46**, 1468 (1992).
[5] C. M. Bowden and J. P. Dowling, Phys. Rev. A **47**, 1247 (1993); **49**, 1514 (1994).
[6] J. J. Maki, M. S. Malcuit, J. E. Sipe, and R. W. Boyd, Phys. Rev. Lett. **67**, 972 (1991).
[7] R. Friedberg, S. R. Hartmann, and J. T. Manassah, Phys. Rev. A **40**, 2446 (1989); R. R. Moseley, B. D. Sinclair, and M. H. Dunn, Opt. Commun. **108**, 247 (1994).
[8] A. S. Manka, J. P. Dowling, C. M. Bowden, and M. Fleischhauer, Phys. Rev. Lett. **73**, 1789 (1994); **74**, 4965 (1995).
[9] N. Wang and H. Rabitz, Phys. Rev. A **52**, 17 (1995).
[10] N. Wang and H. Rabitz, Phys. Rev. A **53**, 1879 (1996).
[11] N. Wang and H. Rabitz (unpublished).
[12] C. M. Bowden, S. Singh, and G. P. Agrawal, J. Mod. Opt. **42**, 101 (1995).
[13] M. Fleischhauer and M. O. Scully, Phys. Rev. A **49**, 1973 (1994).